Rice University

Observation of antiferromagnetic correlations in the Fermi-Hubbad model

by

Pedro M Duarte

A Thesis Submitted
in Partial Fulfillment of the
Requirements for the Degree

Doctor of Philosophy

Approved, Thesis Committee:

Randall G. Hulet, *Chair*
Fayez Sarofim Professor of Physics and Astronomy

Thomas. C. Killian
Professor of Physics and Astronomy

Somebody Else
Professor of Physics and Astronomy

Houston, Texas
December 2012

Abstract

Observation of antiferromagnetic correlations in the Fermi-Hubbad model

by

Pedro M Duarte

Abstract goes here.

Acknowledgements

Acknowledgements go here.

Table of Contents

1 Many body physics with ultracold atoms **1**

1.1 Motivation: Strongly correlated materials 1

1.2 Quantum simulations with ultracold atoms 3

1.3 Quantum magnetism with ultracold atoms 5

1.4 This thesis 8

1.5 Outline 8

2 Ultracold atoms in optical lattices **9**

2.1 One-dimensional optical lattice potential 9

2.1.1 Band structure 11

2.1.2 Eigenstates 12

2.1.3 Wannier states 12

2.2 Three-dimensional optical lattice potential 15

2.3 Hubbard hamiltonian 15

2.3.1 Second quantization 17

2.3.2 Operators in second quantization 20

2.3.3 Second quantized Hubbard hamiltonian 22

2.3.4 Interactions between the atoms 29

3 The Fermi-Hubbard model **30**

3.1 Simplified treatements 30

3.1.1 Exact diagonalization 31

3.1.2 Limiting cases . . . 31
3.1.3 High-temperature series expansion . . . 31
3.1.4 Local density approximation . . . 34
3.1.5 Modern approaches . . . 36

4 Enlarging and cooling towards the Neel state in a compensated optical lattice potential 38

4.1 Compensated optical lattice . . . 38
4.2 Thermodynamic quantitites in the local density approximation . . . 38

5 Experimental diagnostic tools 39

5.1 Absorption imaging . . . 39
5.2 Polarization phase-contrast imaging . . . 39
5.3 Thermometry of a Fermi gas trapped in a harmonic potential . . . 39
5.4 Double occupancy measurement in an optical lattice . . . 39
5.5 Bragg Scattering of light . . . 39
5.5.1 Non-spin sensitive: crystal structure factor . . . 39
5.5.2 Spin sensitive: spin-structure factor . . . 39

6 Experimental setup and procedures 40

6.1 Production of a deeply degenerate ^{6}Li spin mixture in a dimple potential . 40
6.2 Compensated optical lattice potential . . . 40

7 Studies in a three dimensional optical lattice 41

7.1 Determination of the crystal structure factor using Bragg scattering . . . 41
7.2 Insulating states in an uncompensated lattice . . . 41
7.3 Evaporative cooling in a compensated optical lattice . . . 41

Chapter Page

7.4 Detection of antiferromagnetic correlations in a compensated optical lattice 41

8 Conclusion 42

BIBLIOGRAPHY 43

1.1 Motivation: Strongly correlated materials

Our experiences in the physical world can, for the most part, be explained by considering the description of the collections of positively charged nuclei and negatively charged electrons that make up ordinary matter. From high to low energy this includes: neutral plasmas, the formation of free atoms and molecules, the condensation of these atoms and molecules into liquid or glassy phases and their subsequent crystallization to form solids. At lower energies more exotic phenomena take place, starting with magnetism and going further to superfluidity, superconductivity and the novel examples of modern condensed matter physics such as the fractional quantum Hall effect, heavy electrons, high-temperature superconductors and topological insulators.

In principle, the correct description of all the above phenomena is contained in the Schrödinger equation for the interacting system of electrons and nuclei, where the interaction is given by the Coulomb potential. In practice, we know that even though stating the equation is easy, there is not sufficient computing power available in the world to solve it for systems of more than just a few particles. Xiao-Gang Wen, in the introduction to his book [1], points out that back in the 80's a computer with 32 MB of RAM could solve a sytem of 11 interacting electrons. In the 2000's, while computing power has increased more than 100 times, this allows for the addition of only two more electrons to the system.

Despite the above, the use of the Schrödinger equation and perturbation theory for the description of systems of electrons and nuclei has been very succesful over the past century. The most prominent example of this success is our understanding of semiconductors, which are at the root of the electronic devices that permeate all aspects of our lives. The remarkable success of this approach can be traced back to the principle of adiabatic conti-

nuity [2]. This principle states that the low-energy excitations of an interacting system are **non-interacting quasi-particles** which can be closely related to the actual particles that form the interacting system. This last sentence may sound confusing, but think about how a hole in the valence band of a semiconductor (the valence band is a Coulomb interacting Fermi sea of electrons) acts almost like a free, non-interacting positively charged electron.

The practical consequence of adiabatic continuity is that interactions seemingly do not play an important role in the low-energy description of the system. For this reason, the free electron model of Drude and Sommerfeld [3] is relatively succesful in explaining electrical and thermal conductivity in metals, and also in explaining the Hall effect. In 1957, Landau formulated the theory of the Fermi-Liquid [4] and gave a solid basis to the notion of adiabatically connected quasiparticles. To this day, the Fermi-Liquid theory is the starting point for the study of Fermi systems such as conventional metals, helium-3, and ultracold atomic Fermi gases.

But, just as Fermi-Liquid theory is celebrated for its success it is also known for the phenomena that it fails to explain. Starting in the mid 70's and going through the 80's, the discoveries of heavy electron superconductivity [5, 6], the fractional quantum Hall effect [7, 8], and high-temperature superconductors [9] sparked a revolution in condensed matter physics [10]. These class of materials, in which the electron behavior cannot be described effectively in terms of non-interacting electron-like quasiparticles came to be known as **strongly correlated materials**. Strongly correlated materials, and the concept of emergence, introduced by P.W. Anderson in his famous essay "More is Different" [11], are at the center of modern condensed matter physics.

The behavior of strongly correlated materials is emergent because the low-energy excitations of the system bear no resemblance to its constituent particles. This disconnect should not be so surprising, after all we are familiar with this definition of emergence whenever a system undergoes a phase transition. For example when a liquid cools down to form a crystalline solid, translational symmetry is broken. The low-energy excitations of the crys-

tal are the quasiparticles known as phonons, which bear no resemblance to the constituent ions and electrons that form the solid.

Strongly correlated materials are examples of emergent phenomena in which the origin and properties of the low-energy excitations are not as straightforward as those of phonons in a crystalline solid. The fractional quantum Hall state, in which the quasiparticles carry a rational fraction of the charge of an electron serves to illustrate this point. The strong interactions between the electrons in the quantum Hall system (electrons confined in a plane under a very high magnetic field) make the problem intractable from the perturbative point of view and thus **the connection between the microscopic degrees of freedom and the collective low-energy excitations is very difficult to establish**; certainly not as easy as the connection between the small motion of ions about their equillibrium points in the crystal lattice and their collective phonon modes. It was Laughlin's insight that led him to postulate the correct wavefunction for the quantum Hall state [8], but the microscopic origin of the state is still under debate.

The challenge posed by strongly correlated materials has led to great discoveries in condensed matter physiccs, such as the concepts of topological order [12] and quantum criticality [13, 14], but also many questions remain unanswered. Furthermore, the problem of strongly correlated materials is only scratching the surface of what is possible and what remains to be discovered. New materials are being synthesized constantly, and among the myriad of possible materials and compunds yet to be explored by materials scientists, one can only expect that there will be new states of matter to be found; states with technological implications that will revolutionize life on earth.

1.2 Quantum simulations with ultracold atoms

We have seen that, even though the Schrödinger equation in principle contains a full description of a solid, the solution is practically impossible to compute using a classical computer due to the large memory required to represent a many-body quantum state. The approach in condensed matter theory, rather than directly aim to solve the Schrödinger

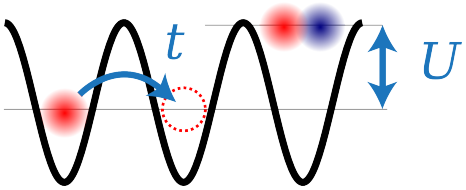

Figure 1.1: Illustration of the Hubbard model

equation, is to introduce simplified effective models, which should capture the essential features of the system under study. The solution of the effective model leads to an understanding of the low-energy excitations of the system and gives clues to their microscopic origin.

The Hubbard model is a model that contains only the essential ingredients to describe the behavior of strongly interacting electrons in a crystalline solid. The model describes electrons that can hop between sites in a lattice (with amplitude t) , and which acquire an interaction energy (U) when two electrons are on the same site, see Figure 1.1. In the next chapter I will explain why this is a plausible model to describe some strongly correlated materials; for now I will point out that even though this model is the simplest possible model for strong correlations, its solution in more than one dimension has evaded theorists for more than four decades [15].

It is at this point that ultracold atoms enter the picture. It turns out that a system of ultracold atoms in an optical lattice is a faithful realization of the Hubbard model [16], and so the properties exhibited by the atoms are in fact the solutions of the model. In this way, the system of atoms in the optical lattice can be used to map the phases and phase boundaries of the Hubbard model in what is known as **quantum simulation**, an idea that was first proposed by Richard Feynman in 1982 [17].

In a seminal paper [16], Jaksch and collaborators showed that Bose-Einstein condensates of atoms loaded into optical lattices could be used as simulators of the Bose-Hubbard model. A few years later the superfluid (SF) to Mott insulator (MI) phase transition, the hallmark of the Bose-Hubbard model, was realized experimentally [18] and several detailed studies

of these system have followed since then [19–23]. For bosonic systems the properties of the ground state are well understood theoretically [24–26]; however experiments of atoms in lattices are starting to shed light into the dynamics of these systems [27], which are more difficult to address theoretically.

Despite the remarkable advances with bosonic systems, the ultimate goal of quantum simulation with ultracold atoms is to find the ground states of theoretically intractable models, to see if these models can reproduce the measured properties of strongly correlated electron systems. In this prescription for quantum simulation, the subject of most interest is the Hubbard model and whether it can exhibit a d-wave superfluid state which would validate it as the prime model for high temperature superconductors. In pursuit of this goal, experiments have realized the Hubbard model with fermionic atoms, populating two hyperfine levels of the ground state which play the role of spin-up and spin-down states of spin-$\frac{1}{2}$ electrons. The spin-mixture of atoms is loaded in a periodic optical lattice potential. The lattice depth and the contact interactions between the atoms, which set the values for the Hubbard parameters t and U, can be controlled almost at will by the experimeter. The lattice depth is adjusted with lattice laser power, and the interactions are controlled using a magnetically tunable Feshbach resonance, offering the possiblity of realizing non-interacting samples, or samples with attractive or repulsive interactions. These unprecedented control over the system parameters has allowed the realization of band insulating states [28] and Mott insulating states [29, 30]. However, the possibility of exploring the strongly correlated phases of the Hubbard model is still distant because the required temperatures are out of reach for current experiments.

1.3 Quantum magnetism with ultracold atoms

Even though temperatures as low as $T = 0.05T_F$ can be reached with ultracold Fermi gases, these temperatures are not low enough to allow exploration of the strongly correlated phases of the Hubbard model. To get an idea of the energy scales required we will examine a

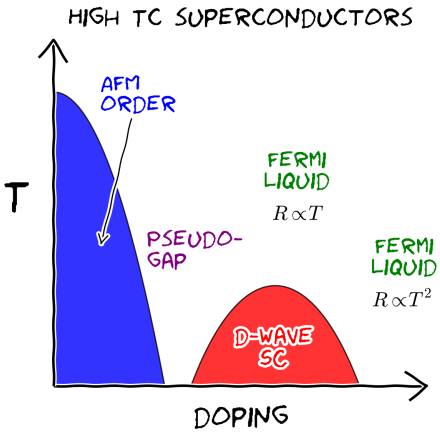

Figure 1.2: Cartoon phase diagram for cuprate high-T_C superconductors. The anitiferromagnetic insulator (AFM) and the Fermi liquid with quadratic resistivity are well understood by theory, however the strange Fermi liquid with linear resistivity and the interplay between the pseudogap regime and the superconducting dome are issues still under debate [34].

qualitative temperature-doping (T-x) phase diagram, which can be obtained experimentally for the cuprate high-temperature superconductors (HTS)[1], see Fig. 1.2.

The cartoon phase diagram shown in Fig. 1.2 shows that HTS's exhibit various interesting phases besides the superconducting (SC) dome at intermediate doping. Most importantly, the undoped parent compund is an antiferromagnet with a Néel ordering temperature that is higher than any T_C along the SC dome.

In $YBa_2Cu_3O_{6+x}$ (the most common HTS [35] also usually referred to just as YBCO), superconductivity at a temperature as large as 93 K is obtained for optimal hole-doping [36]. The parent compund, where the doping is $x = 0$, is antiferromagnetic with a Néel temperature $T_N \approx 500K$ [37]. The Fermi energy for this compound is on the order of ~ 4 eV [38], which corresponds to ~ 40000 K. The critical temperature for superconductivity is then $T_C \sim 0.002 T_F$; however the Néel temperature of the parent compund is higher at $T_N \sim 0.012$

State of the art temperatures for ultracold atoms trapped in a harmonic potential are $\sim 0.05\, T_F$. Of course, the system of ultracold atoms is isolated from the environment and not

[1] See [31] for a review, [32] for a study of the onset of superconductivity at optimal hole-doping, [33] for the phase diagram of hole-doped superconductors and [34] for a more accessible report on the subject.

in contact with a thermal reservoir, so when loaded into the optical lattice its temperature can change adiabatically. For resonable values of t and U in the lattice, the adiabatic change of the temperature is typically less than an order of magnitude, and sometimes can even lead to larger values of T/T_F in the lattice [39]. So by comparison with the critical temperature of $0.002T_F$ for the HTS's we see that ultracold atoms are still too hot to realize strongly correlated phases.

Even though we cannot reach the temperatures required to realize a full quantum simulation of the Hubbard model, that does not mean we pack and go home. As we saw in the above phase diagram, the Néel antiferromagnetically (AFM) orderered state which is present in an undoped sample occurs at a much higher temperature. Immediately after a Mott insulating state of fermionic atoms in a simple cubic lattice was first produced back in 2008 [29, 30], the race started to see which group could be the first to observe the AFM state and take the next step in the roadmap of quantum simulation.

At the origin of the AFM state is the exchange energy that arises due to the Pauli exclusion principle, the hopping of atoms from site to site, and their interactions [40]. In Ising type models, the magnetic coupling (anti or ferromagnetic) is put in by hand in the Hamiltonian, but in the Hubbard model it arises naturally, like it does in real magnets, from the exchange interaction. Since the exchange interaction is a purely quantum mechanical effect, any phenomena that is a consequence of it forms part of the general concept of **quantum magnetism**.

Recently in 2013, the Esslinger group has demonstrated a way of using a dimerized optical lattice to measure the nearest neighbor spin correlations that start to develop as a consequence of the exchange interaction at temperatures a few times larger than the Néel temperature for AFM ordering [41]. They observe significant spin-spin correlations in arrays of 1D chains and they can detect the spin-spin correlations that form on the approach to AFM order in a simple cubic lattice. Prior to the work of Esslinger, the Bloch group used a similar dimerized optical lattice to study exchange interactions with bosons in isolated

double-wells [42].

The AFM state, besides being the natural stepping stone in the quest to simulating strongly correlated systems, offers the added benefit that is a state that is well understood by theory [43, 44]. The absence of doping in the condensed matter system is equivalent to having a density of one atom per site in the ultracold atom system. The energy band has a total capacity of two atoms per site, so this $x = 0$ point in the phase-diagram is also referred to as half-filling. At half-filling, numerical approaches to the Hubbard model, such as quantum Motnte Carlo (QMC) [43], and dynamical mean field theory (DMFT) [44] do not suffer from the Fermion sign problem [45], and calculations can be performed down to temperatures below the Néel temperature for AFM ordering.

The ability to compare experimental results with theory offers a testbed for quantum simulation. Once the details are worked out, the AFM state at half-filling ($x = 0$) is going to be the basis of a thermometer for measurements of the strongly correlated phses of the Hubbard model. So the challenge for our experiments is two-fold: temperatures in fermionic systems still have to be lowered to reach the Néel temparature, and the methods to use the AFM state and comparison with theory to define a universal thermometer have to be established.

1.4 This thesis

Over the course of this work we have used a compensated lattice potential to explore the idea of entropy redistribution and how it may help reach the Néel state at the core of an inhomogeneous gas [43]. In addition to that we have implemented a technique to measure the spin structure factor of the inhomogeneous sample using Bragg scattering of light. These two techniques directly address the issues of cooling and thermometry which at the moment are the biggest roadblock for the advancement of quantum simulation [46]

1.5 Outline

In this chapter we consider the description of cold atoms in an optical lattice potential. Second quantization is introduced, and the many-body Hubbard hamiltonian is derived. We also disuss the requirements necessary for a system to be well described by a single band Hubbard model.

2.1 One-dimensional optical lattice potential

The contents of this section follow the derivation found in § IV A of the review article by Morsch and Oberthaler. [47]. The hamiltonian for an atom moving in a 1D lattice potential is

$$H_{\text{single,1D}} = -\frac{\hbar^2}{2m}\frac{\partial^2}{\partial x^2} + V_0 \sin^2(kx) \tag{2.1}$$

where $k = 2\pi/\lambda$, and λ is the wavelength of the lattice laser. The lattice spacing is $a = \lambda/2$. If V_0 is in units of the recoil energy $E_R = \frac{\hbar^2 k^2}{2m}$, then the hamiltonian can be written as

$$\begin{aligned} H_{\text{single,1D}} &= -\frac{1}{k^2}\frac{\partial^2}{\partial x^2} + V_0 \sin^2(kx) \\ H_{\text{single,1D}} &= -\frac{1}{k^2}\frac{\partial^2}{\partial x^2} + \frac{V_0}{4}(2 - e^{2ikx} - e^{-2ikx}) \end{aligned} \tag{2.2}$$

The solution to this equation can be found in terms of Bloch states, which are labeled by their quasimomentum q, and their band index n

$$\psi_q^n(x) = e^{iqx} \sum_{m\in\mathbb{Z}} c_{qm}^n e^{imGx} \tag{2.3}$$

The lattice translation invariant function that typically accompanies e^{iqx} has been written here as a sum of plane waves (labeled by the integer m) at the reciprocal lattice vectors. This is the Fourier series of any such periodic function and represents no loss of generality. The reciprocal lattice vector $G = \frac{2\pi}{a} = 2k$, where $a = \lambda/2$ is the lattice spacing.

Plugging the Bloch states into the hamiltonian and then rearranging some of the terms in the infinite sum, we get

$$\begin{aligned} H_{\text{single,1D}}\psi_q(x) &= \sum_m \left[(q/k+2m)^2 + \frac{V_0}{4}(2-e^{2ikx}-e^{-2ikx})\right] c_{qm}^n e^{iqx+im2kx} \\ H_{\text{single,1D}}\psi_q(x) &= \sum_m \left[\left((q/k+2m)^2+\frac{V_0}{2}\right)c_{qm}^n - \frac{V_0}{4}c_{q,m-1}^n - \frac{V_0}{4}c_{q,m+1}^n\right] e^{iqx+im2kx} \end{aligned} \tag{2.4}$$

The left hand side of the time-independent Schrodinger equation is simply

$$E_q^n\psi_q(x) = \sum_m E_q c_{qm}^n e^{iqx+imGx} \tag{2.5}$$

For the coefficients c_{qm}^n to represent an eigenstate of the problem, the Bloch state needs to satisfy $H\psi_q(x) = E_q^n\psi_q(x)$, and since the plane waves are linearly independent functions this means that

$$\left((q/k+2m)^2+\frac{V_0}{2}\right)c_{qm}^n - \frac{V_0}{4}c_{q,m-1}^n - \frac{V_0}{4}c_{q,m+1}^n = E_q c_{qm}^n \tag{2.6}$$

The quasimomentum is restricted to the first Brillouin zone, which can be taken to be between $[-\frac{\pi}{a},\frac{\pi}{a})$ or between $[0,\frac{2\pi}{a})$. We will express the quasimomentum in units of $\frac{2\pi}{a}=2\pi$, so in the equation above we will make the replacement $q/k \to 2q$. Also in the equation for the Bloch state $q \to 2\pi q$

We then have a linear system of equations which determines the c_{qm}^n. The number of equations is infinite, but for our practical purposes we will truncate it such that $|m| < \mathcal{N}$. The resulting equations can be written in matrix form, for example if we select $\mathcal{N}=2$

$$\begin{bmatrix} \frac{1}{2}V_0+4(q-2)^2 & -\frac{1}{4}V_0 & 0 & 0 & 0 \\ -\frac{1}{4}V_0 & \frac{1}{2}V_0+4(q-1)^2 & -\frac{1}{4}V_0 & 0 & 0 \\ 0 & -\frac{1}{4}V_0 & \frac{1}{2}V_0+4q^2 & -\frac{1}{4}V_0 & 0 \\ 0 & 0 & -\frac{1}{4}V_0 & \frac{1}{2}V_0+4(q+1)^2 & -\frac{1}{4}V_0 \\ 0 & 0 & 0 & -\frac{1}{4}V_0 & \frac{1}{2}V_0+4(q+2)^2 \end{bmatrix} \tag{2.7}$$

In the numerical solution that we implemented we chose $\mathcal{N}=5$, it turns out that to accurately obtain the dispersion relationship for the n^{th} band you pretty much only need $\mathcal{N}=n+1$, so using $\mathcal{N}=5$ is somewhat overkill for us since we will be mostly concentrated on the lowest band and the first excited band.

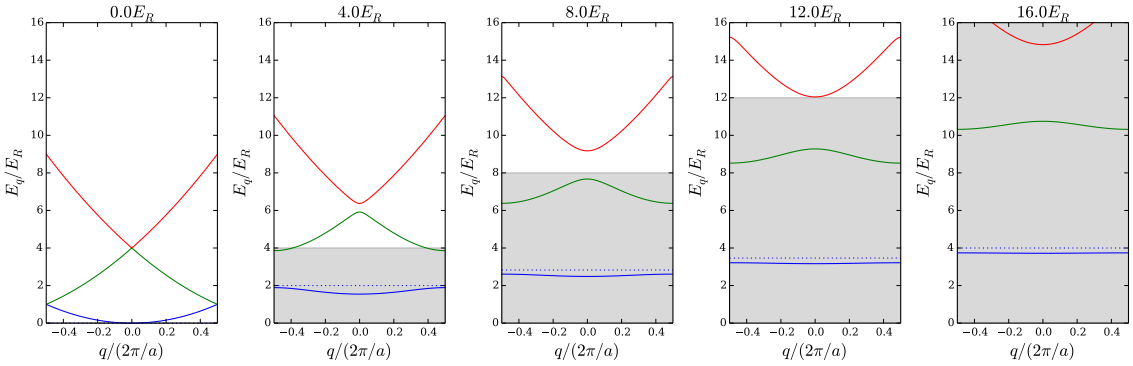

Figure 2.1: Band structure in a 1D optical lattice. The depth of the lattice is indicated by the shaded area, and the energy of the hamonic oscillator ground state in a single lattice site is shown as a dotted line.

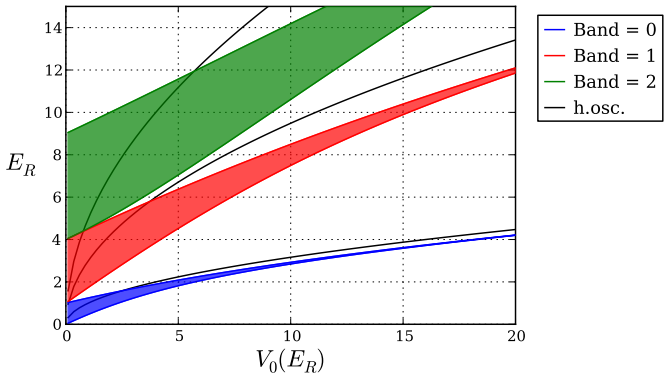

Figure 2.2: Band structure in a 1D optical lattice. Each band is indicated by the colored area, the harmonic oscillator states in an isolated lattice site are shown as black lines.

2.1.1 Band structure

We can find the solutions for the set of coefficients c^n_{qm} by diagonalizing the matrix shown above. The eigenvalues correspond to the energies E^n_q as a function of quasimomentum q and band index n, this set of solutions is referred to as the band structure, and we show it for a 1D lattice as a function of q in Fig. 2.1, and also as a function of lattice depth in Fig. 2.2

We mention here that the Schrodinger equation for the hamiltonian in Eq. 2.1, has solutions called Mathieu functions. One can calculate the band structure by using the

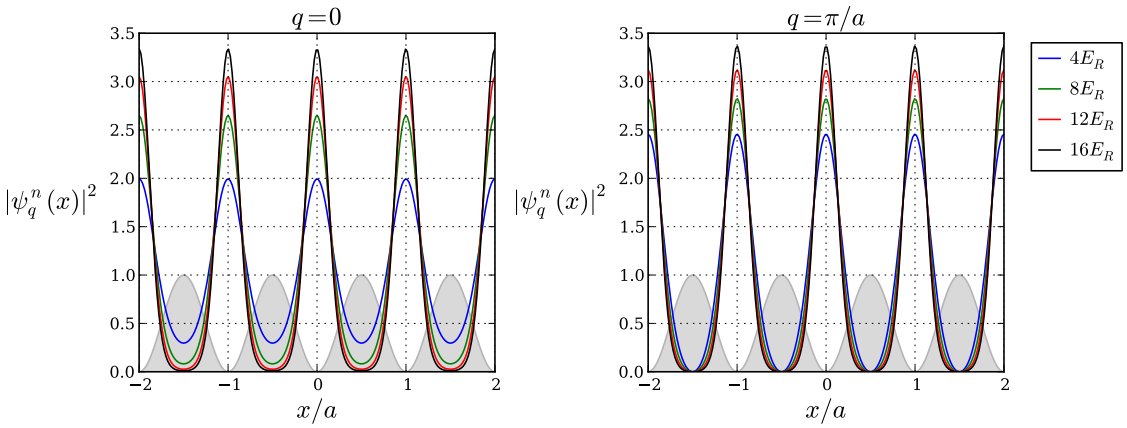

Figure 2.3: Eigenstates of the Hamiltonian in a 1D optical lattice shown for $q = 0$ (left) and $q = \pi/a$ (right) for various lattice depths. The states are normalized so that the integral of the probability density over one lattice site is equal to one. The gray shaded region is shown to indicate the variation of the lattice potential.

known properties of the Mathieu functions, which are avaiable on tables or as functions in some softare packages (e.g. Mathematica), see for instance the treatement in [48].

2.1.2 Eigenstates

For each energy eigenvalue we have an associated eigenstate which is defined in terms of the c_{qm}^n by Eq. 2.3. Typically, numerical diagonalization routines return the normalized eigenvectors of the matrix in question, and for us this means that the coefficients c_{qm}^n will satisfy

$$\sum_m |c_{qm}^n|^2 = 1 \tag{2.8}$$

This has the implication that the states obtained from Eq. 2.3 will be normalized over a lattice site. In Fig. 2.3. we show the probability density for a lowest band eigenstate as a function of position in the lattice for various lattice depths. One can see how, as the lattice gets deeper, the state becomes more localized around the center of each lattice site.

2.1.3 Wannier states

It is useful to define a basis of states that are localized around a single lattice site. We will see later on that when using such a basis the hamiltonian for the Hubbard model

takes its most familiar form. The localized states, centered around the site at x_j, can be constructed as the following superposition of eigenstates of the hamiltonian [1]

$$w^n(x - x_j) = \frac{1}{L} \sum_q e^{-iq2\pi x_j} \psi_q^n(x) \tag{2.9}$$

Here we have considered a finite sized lattice with a total of L sites. We use the set of unique quasimomenta defined by $q = \frac{2\pi n}{a}$ $\forall n \in \{0, 1, \dots L-1\}$. The definition of this set is arbitrary, but there is no loss of generality. This becomes clear we insert the expansion of $\psi_q^n(x)$ in plane waves into the definition of the Wannier state.

$$w^n(x - x_j) \equiv w_j^n(x) = \frac{1}{L} \sum_q \sum_{m \in \mathbb{Z}} c_{qm}^n e^{-i2\pi q x_j} e^{i2\pi(q+m)x} \tag{2.10}$$

The Wannier state is a sum of plane waves, and all plane waves will be covered, regardless of the set of unique quasimomenta that we decide to consider, since m runs over all integers. We will set $x_j = 0$ for the calculation of the Wannier function. WWannier states centered at different lattice sites can be obtained by translation of the $x_j = 0$ solution.

$$w_0^n(x) = \frac{1}{L} \sum_q \sum_{m \in \mathbb{Z}} c_{qm}^n e^{i2\pi(q+m)x} \tag{2.11}$$

Since the hamiltonian communtes with the parity operator it is required that $\psi_q^n(-x) = \pm\psi_q^n(x)$ which implies that $c_{qm}^n = \pm c_{q'm'}^n$ if $(q+m) = -(q'+m')$. Then, the Wannier state becomes

$$w_0^n(x) = \frac{1}{L} \left(c_{00}^n + \sum_{q>0} \sum_{m>0} c_{qm}^n \left[e^{i2\pi(q+m)x} \pm e^{-i2\pi(q+m)x} \right] \right) \tag{2.12}$$

It is shown in [50] that the maximally localized Wannier states are obtained if the plus sign is chosen for even bands and the minus sing is chosen for odd bands. So, the Wannier states are symmetric for the even bands and antisymmetric for the odd bands.

$$w_0^n(x) = \frac{c_{00}^n}{L} + \frac{2}{L} \sum_{q>0} \sum_{m>0} c_{qm}^n \begin{cases} \cos[2\pi(q+m)x] & \text{if } n \text{ even} \\ \sin[2\pi(q+m)x] & \text{if } n \text{ odd} \end{cases} \tag{2.13}$$

[1] In some treatments (for instance [49]) the Wannier function is defined with a normalization factor of $\sqrt{N_s}$ rather than N_s as shown here. This is considering eigenfunctions $\psi_q^n(x)$ which are normalized when integrating over the full extent in the lattice. We stick to the N_s normalization factor, without the square root, since the eigenfunctions that are obtained numerically come out normalized over a lattice site, as was explained in the previous section.

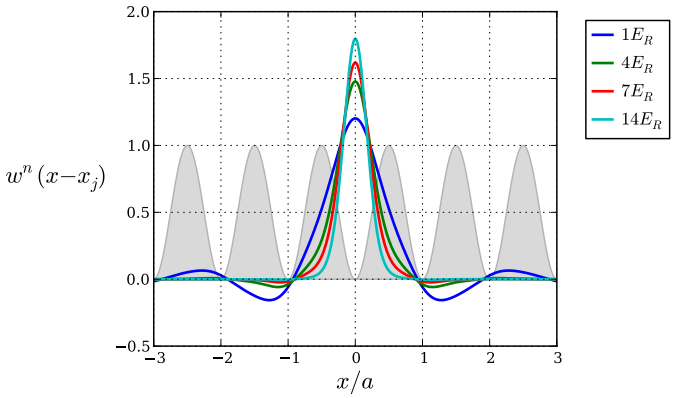

Figure 2.4: Localized Wannier states in a 1D optical lattice for various lattice depths. The gray shaded region is shown to indicate the spatial variation of the lattice potential.

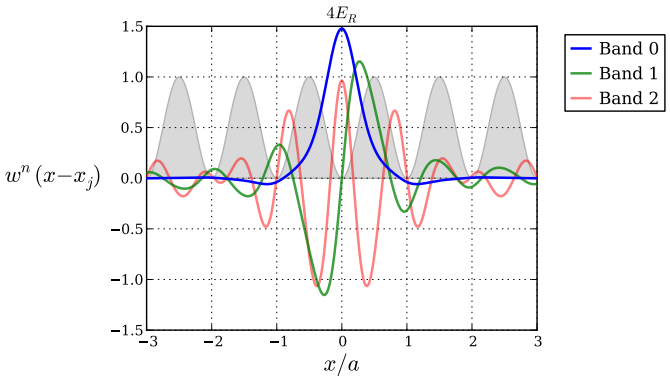

Figure 2.5: Localized Wannier states in a $4E_R$ 1D optical lattice for the first three energy bands. The gray shaded region is shown to indicate the spatial variation of the lattice potential.

For $q, m > 0$ all the coefficients c^n_{qm} will have the same sign, so we select them to be positive.

We can now proceed to add up the plane waves to obtain the Wannier states which are shown in Fig. 2.4 for various lattice depths. As the lattice depth is increased, the Wannier states become more localized. This leads to less overlap betweeen Wannier states in adjacent sites, which results in a reduction of the amplitude for a particle to tunnel from one site to the next one. More localized states also imply that the on-site interaction will be larger, since two particles in the same site will be closer to each other on average.

In Fig. 2.5 we show the Wannier functions for the first three bands in a $4E_R$ lattice.

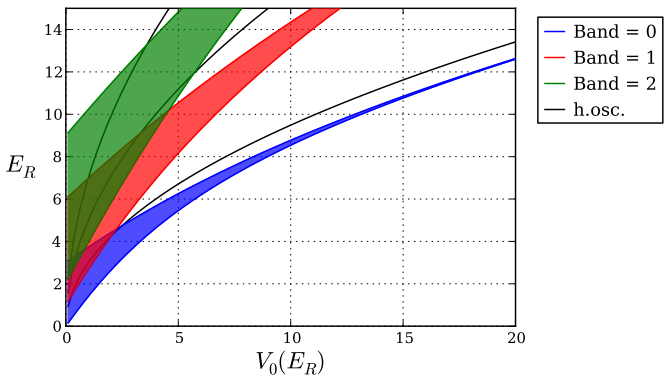

Figure 2.6: Band structure in a 3D optical lattice. Each band is indicated by the colored area, the harmonic oscillator states in an isolated lattice site are shown as black lines.

2.2 Three-dimensional optical lattice potential

The hamiltonian for an atom moving in a 3D lattice can be separated in the three spatial coordinates. So we can use the solutions that were obtained in the previous section for the 1D lattice and obtain the band structure and the Wannier states for the 3D lattice. The band structure is shown in Fig. 2.6.

The Wannier states in a 3D lattice are simply products of the Wannier states in each of the three spatial coordinates. They are defined as

$$w^n(\boldsymbol{r}-\boldsymbol{r}_j) = \frac{1}{L^3}\sum_{\boldsymbol{q}} e^{-i\boldsymbol{q}\cdot\boldsymbol{r}_j} \prod_{u=x,y,z} \psi_{q_u}^{n_u}(u) \tag{2.14}$$

where L^3 is the total number of sites in the lattice.

2.3 Hubbard hamiltonian

The many-body Hubbard hamiltonian is

$$H = -t\sum_{\langle ij\rangle,\sigma} a_{i\sigma}^\dagger a_{j\sigma} + U\sum_i n_{i\uparrow}n_{i\downarrow} \tag{2.15}$$

In what follows we will see how to obtain this many-body form starting from the first quantized version of the hamiltonian for a system of N particles.

The hamiltonian for a single atom in a 3D optical lattice is given by

$$H_{\text{single,3D}} = -\frac{\hbar^2}{2m}\left(\frac{\partial^2}{\partial x^2}+\frac{\partial^2}{\partial y^2}+\frac{\partial^2}{\partial z^2}\right)+V_0\left(\cos^2(kx)+\cos^2(ky)+\cos^2(kz)\right) \tag{2.16}$$

and when N particles are considered, along with their interactions the hamiltonian takes a more complicated form

$$\begin{aligned} H =& \sum_l^N \left[-\frac{\hbar^2}{2m}\left(\frac{\partial^2}{\partial x_l^2}+\frac{\partial^2}{\partial y_l^2}+\frac{\partial^2}{\partial z_l^2}\right)+V_0\left(\cos^2(kx_l)+\cos^2(ky_l)+\cos^2(kz_l)\right)\right] \\ &+\frac{1}{2}\sum_{l,m,l\neq m}^N V_{\text{int}}(\boldsymbol{r}_l,\boldsymbol{r}_m) \\ =& H_0+H_{\text{int}} \end{aligned} \tag{2.17}$$

where the particles are labeled by indices l,m, and V_{int} is the potential energy of interaction between two partcles. In the last line we have defined the more concise notation that splits the Hamiltonian into the non-interacting (H_0) and the interacting (H_{int}) parts. Solving this problem is a daunting task primarily for two reasons:

1. The Bose or Fermi statistics of the identical particles under consideration require the wavefunctions to be symmetrized or antysymmetrized products of single-particle wavefunctions.

2. The interactions between the particles prevent a straightforward reformulation of the problem as a collection of easier-to-solve single particle hamiltonians.

The formalism of many-body theory encapsulates a series of methods to deal with the two issues mentioned above. First, the reformulation of the Schrodinger equation in the language of second quantization provides the advantage that the statistics are automatically taken into account by the notation, so one can essentially forget about the the (anti)symmetrization of the many-particle wave functions. The small price to pay is that one needs to be very careful and consistent about the order in which operators show up in the notation, since the symmetry properties of the resulting states are contained in the commutation relations defined between the operators. Furthermore, second quantization

makes it easy to consider the extended Hilbert space where the number of particles is not fixed, this is known as Fock space.

For weak interactions, many-body theory provides a solution to the problem in terms of perturbation expansions for the physical quantities of interest. The theoretical formalism also reduces most of the important physical quantities in terms of certain matrix elements (Green's functions) which allows the user to concentrate on obtaining such matrix elements which serve as a starting point for the exploration of the properties of any system. The complication arises when the interactions are not weak, and the perturbative approach of the many-body formalism breaks down. For this reason, the Hubbard model with strong interactions (we will quantify the definition of strong later on) has been a major challenge for theoretical physicists over the last four decades.

2.3.1 Second quantization

The contents of this section follow the treatment in the books by Fetter and Walecka [51] and Schwabl [52].

Let's start with a complete orthonormal set of single particle states $\{|i\rangle\} = \{|1\rangle, |2\rangle, \ldots\}$, using these states we can write the basis states for the N-particle system as

$$|i_1, \ldots i_\alpha, \ldots i_N\rangle \tag{2.18}$$

which represents a state in which particle 1 is in state $i_1 \in \{|i\rangle\}$, particle α is in state i_α and so on. These product states are not eigenstates of the permutation operator P_{ij} which interchanges particles i and j. However, starting from the product states we can obtain the symmetrized (bosons) and antisymmetrized (fermions) normalized basis states.

For bosons the normalized symmetrized states are

$$|n_1, n_2, \ldots\rangle = \frac{1}{\sqrt{N! n_1! n_2! \ldots}} \sum_P P|i_1, i_2, \ldots i_N\rangle \tag{2.19}$$

where the sum over P runs over all $N!$ elements of the permutation group for N objects. In this expression, n_1 is the number of times that the state $|1\rangle$ occurs among the N particles,

or in other words, n_1 is the number of particles in state $|1\rangle$. The sum of all occupation numbers n_i must equal the total number of particles, but otherwise there is no restriction in the occupation number for bosons.

For fermions the normalized antysymmetrized states are written in the form of Slater determinants:

$$\begin{aligned} |n_1, n_2, \ldots\rangle =& \frac{1}{\sqrt{N!}} \sum_P (-1)^P P |i_1, i_2, \ldots i_N\rangle \\ =& \frac{1}{\sqrt{N!}} \begin{vmatrix} |i_1\rangle_1 & |i_1\rangle_2 & \cdots & |i_1\rangle_N \\ \vdots & \vdots & \ddots & \vdots \\ |i_N\rangle_1 & |i_N\rangle_2 & \cdots & |i_N\rangle_N \end{vmatrix} \end{aligned} \tag{2.20}$$

In this case, the product states are multiplied by -1 for odd permutations, and the occupation numbers n_i can only take the values 0 or 1.

For both bosons and fermions, we can combine the states for $N = 0, 1, 2, \ldots$ particles to obtain a complete orthonormal set of states for arbitrary particle number. This set of states, which are referred to as number states, spans what is called the Fock space.

We now define the creation operators for bosons, which allow us to take a state from the subspace of N particles, to the subspace of $N + 1$ particles.

$$a_i^\dagger |\ldots, n_i, \ldots\rangle = \sqrt{n_i + 1} |\ldots, n_i + 1, \ldots\rangle \tag{2.21}$$

It follows that the adjoint of the creation operator is the annihilation operator and satisfies

$$a_i |\ldots, n_i, \ldots\rangle = \begin{cases} \sqrt{n_i} |\ldots, n_i - 1, \ldots\rangle & \text{if } n_i \geq 0, \\ 0 & \text{if } n_i = 0 \end{cases} \tag{2.22}$$

The creation and annihilation operators are defined such that one can create any state starting from the vacuum state $|0\rangle \equiv |0, 0, \ldots\rangle$ in which there are no particles at all. In more formal terms

$$|n_1, n_2, \ldots\rangle = \frac{1}{\sqrt{n_1! n_2! \ldots}} (a_1^\dagger)^{n_1} (a_2^\dagger)^{n_2} \ldots |0\rangle \tag{2.23}$$

The boson creation and annihilation operators satisfty the Bose communtation relations

$$[a_i, a_j] = 0 \qquad [a_i^\dagger, a_j^\dagger] = 0 \qquad [a_i, a_j^\dagger] = \delta_{ij} \tag{2.24}$$

In the case of fermions we want to also define creation operators such that the number states can be written as in Eq. 2.23. A subtlety arises in the case of fermions since the order in which the creation operators are applied affects the resulting number state[2]. Take the number state defined in Eq. 2.20. If we interchange the state labels 1 and 2 we get

$$\begin{aligned} |n_2, n_1, \ldots\rangle =& \frac{1}{\sqrt{N!}} \sum_P (-1)^P P |i_2, i_1, \ldots i_N\rangle \\ =& -\frac{1}{\sqrt{N!}} \sum_P (-1)^P P |i_1, i_2, \ldots i_N\rangle \\ =& -|n_1, n_2, \ldots\rangle \end{aligned} \tag{2.25}$$

where the minus sign in the second line is a result of the properties of determinants, namely you get a minus sign if you exchange two columns.

If we adopt as a definition of the creation operators the following expression for the number state

$$|n_1, n_2, \ldots\rangle = (a_1^\dagger)^{n_1} (a_2^\dagger)^{n_2} \ldots |0\rangle \quad , \qquad n_i = 0, 1 \tag{2.26}$$

then using the result of Eq. 2.25 above, the fermion creation operators must satisfy the following anticommutation relation

$$a_i^\dagger a_j^\dagger + a_j^\dagger a_i^\dagger \equiv [a_i^\dagger, a_j^\dagger]_+ = 0 \tag{2.27}$$

Notice that this also contains the necessary implication that $(a_i^\dagger)^2 = 0$, which is a manifestation of the Pauli exclusion principle. It follows from here that the creation and annihilation operators for fermions satisfy

$$\begin{aligned} a_i^\dagger |\ldots, n_i, \ldots\rangle =& (1 - n_i)(-1)^{\sum_{k<i} n_k} |\ldots, n_i + 1, \ldots\rangle \\ a_i |\ldots, n_i, \ldots\rangle =& n_i (-1)^{\sum_{k<i} n_k} |\ldots, n_i - 1, \ldots\rangle \end{aligned} \tag{2.28}$$

[2]This is not a problem in bosons which is seen by looking at Eq. 2.23 and recalling that the Bose commutation relations say that all creation operators commute

and also that they satisfy the Fermi anticommutation relations

$$[a_i, a_j]_+ = 0 \qquad [a_i^\dagger, a_j^\dagger]_+ = 0 \qquad [a_i, a_j^\dagger]_+ = \delta_{ij} \tag{2.29}$$

From now on we shall focus on the case of Fermions, since this is the most relevant for our experiment.

2.3.2 Operators in second quantization

So far two great leaps have been taken:

1. We have swept antisymmetrization under the rug by introducing the number states, defined from the vacuum in terms of creation operators wich satisfy the Fermi anti-commutation reations.

2. We started from an N particle hamiltonian, but we have now defined states that can handle the description of systems with an arbitrary number of particles

The two ideas mentioned are related to the states used to describe the system, now we will turn to the problem of the observables and see how they are handled in the second quantization.

Let us consider the following sum over particles $\sum_\alpha |i\rangle_\alpha\langle j|_\alpha$ and apply it to the number states as defined in Eq. 2.20

$$\left(\sum_\alpha |i\rangle_\alpha\langle j|_\alpha\right)|n_1, n_2, \ldots\rangle = \frac{1}{\sqrt{N!}}\sum_P (-1)^P P\left(\sum_\alpha |i\rangle_\alpha\langle j|_\alpha |i_1, i_2, \ldots i_N\rangle\right) \tag{2.30}$$

On the left hand side, for the term in parenthesis not to vanish, there must be one particle in state $|j\rangle$, so we must have $n_j = 1$ in the initial state. Also, since these are fermions, there can be no particles in state $|i\rangle$ in the intitial state, so $n_i = 0$, or else the Slater determinant operator will make the state vanish after applying the $|i\rangle\langle j|$. If the particle initially in state

$|j\rangle$ is labeled as β then the two mentioned conditions can be embodied as

$$\begin{aligned}\left(\sum_\alpha |i\rangle_\alpha\langle j|_\alpha\right)|n_1,n_2,\ldots\rangle =& n_j(1-n_i)\frac{1}{\sqrt{N!}}\sum_P(-1)^P P\left(|i\rangle_\beta \underbrace{|i_1,i_2,\ldots i_N\rangle}_{\text{wihtout } |j\rangle_\beta}\right)\\ =& n_j(1-n_i)\frac{1}{\sqrt{N!}}\begin{vmatrix} |i_1\rangle_1 & |i_1\rangle_2 & \cdots & |i_1\rangle_N\\ \vdots & \vdots & & \vdots\\ |i\rangle_1 & |i\rangle_2 & \cdots & |i\rangle_N\\ \vdots & \vdots & & \vdots\\ |i_N\rangle_1 & |i_N\rangle_2 & \cdots & |i_N\rangle_N\end{vmatrix}\end{aligned} \tag{2.31}$$

In the determinant of the left the state $|i\rangle$ appears in the j^{th} row, so a few rows need to be exchanged to put it in the correct place according to our sign convention for the number states.

$$\begin{aligned}\left(\sum_\alpha |i\rangle_\alpha\langle j|_\alpha\right)|n_1,n_2,\ldots\rangle =& n_j(1-n_i)|\ldots,n_i+1,\ldots,n_j-1,\ldots\rangle\times\begin{cases}(-1)^{\sum_{k<j}n_k+\sum_{k<i}n_k} & \text{if } i\le j,\\ (-1)^{\sum_{k<j}n_k+\sum_{k<i}n_k-1} & \text{if } i>j\end{cases}\\ =& a_i^\dagger a_j|n_1,n_2,\ldots\rangle\end{aligned} \tag{2.32}$$

where the last equality can be obtained by examining the definition of the creating and annihilation operators given above.

After this last step we can establish the important relation

$$\sum_\alpha |i\rangle_\alpha\langle j|_\alpha = a_i^\dagger a_j \tag{2.33}$$

We now turn our attention to the operators in the N-particle system. Consider an operator T that is a sum over single particle operators

$$T=\sum_\alpha t_\alpha \tag{2.34}$$

If we insert the completness relation for the single particle states twice in this sum we have

$$\begin{aligned} T =& \sum_{\alpha} \left(\sum_{i} |i\rangle_\alpha \langle i|_\alpha \right) t_\alpha \left(\sum_{j} |j\rangle_\alpha \langle j|_\alpha \right) \\ =& \sum_{ij} \langle i|t|j\rangle \sum_{\alpha} |i\rangle_\alpha \langle j|_\alpha \\ =& \sum_{ij} \langle i|t|j\rangle a_i^\dagger a_j \equiv \sum_{ij} t_{ij} a_i^\dagger a_j \end{aligned} \tag{2.35}$$

This is the other big leap provided by the second quantization: the operators which were written as a sum over particles now are written as a sum of creation and annihilation operators over single particle states.

Operators like the potential energy, which are a sum over two-particle (or many-particle) operators, can be equally expressed as sums of creation and annihilation operators. For a two-body operator we have the expression

$$\begin{aligned} F =& \frac{1}{2} \sum_{\alpha \neq \beta} f(\boldsymbol{r}_\alpha, \boldsymbol{r}_\beta) \\ =& \frac{1}{2} \sum_{ijkm} \langle ij|f|km\rangle a_i^\dagger a_j^\dagger a_m a_k \end{aligned} \tag{2.36}$$

2.3.3 Second quantized Hubbard hamiltonian

The Hubbard hamiltonian in Eq. 2.17 is a sum of two single-particle operators and one two-particle operator. These are respectively: the kinetic energy, the energy of the atoms in the lattice potential, and the interactions between the atoms. As a single-particle basis we pick the Wannier states that were derived in Section. 2.1.3

In the Hubbard hamiltonian the two single-particle operators are grouped together to define the non-interacting part of the hamiltonian

$$\begin{aligned} H_0 =& \sum_{l}^{N} -\frac{\hbar^2}{2m} \left(\frac{\partial^2}{\partial x_l^2} + \frac{\partial^2}{\partial y_l^2} + \frac{\partial^2}{\partial z_l^2} \right) + V_0 \left(\cos^2(kx_l) + \cos^2(ky_l) + \cos^2(kz_l) \right) \\ =& \sum_{l}^{N} H^l_{\text{single,3D}} \end{aligned} \tag{2.37}$$

Tunneling matrix element, t IMPORTANT NOTE: In this section I have already restricted the set of states to only the Wannier states in the lowest band. I should mention somewhere in this section that this approximation is taking place.

H_0 is a single particle operator, so it's second quantized form is

$$\begin{aligned} H_0 =& \sum_{ij} \langle i|H_{\text{single,3D}}|j\rangle a_i^\dagger a_j \\ =& -\sum_{ij} t_{ij} a_i^\dagger a_j \end{aligned} \tag{2.38}$$

Note that the sign of t_{ij} was picked rather arbitrarily to follow the usual conventions. We now proceed to find the value of the matrix element. We use the definition of the Wannier states given in Eq. 2.14 to find

$$\begin{aligned} -t_{ij} =& \frac{1}{L^6} \int \mathrm{d}\boldsymbol{r} \sum_{\boldsymbol{q}'} e^{i\boldsymbol{q}'\cdot\boldsymbol{r}_i} \prod_{u'=x,y,z} \psi^{n'_{u'}*}_{q'_{u'}}(u') \Big(H_{\text{single,3D}}\Big) \sum_{\boldsymbol{q}} e^{-i\boldsymbol{q}\cdot\boldsymbol{r}_j} \prod_{u=x,y,z} \psi^{n_u}_{q_u}(u) \\ =& \sum_{\boldsymbol{q}\boldsymbol{q}'} \frac{E^n_{\boldsymbol{q}}}{L^6} e^{i\boldsymbol{q}'\cdot\boldsymbol{r}_i} e^{-i\boldsymbol{q}\cdot\boldsymbol{r}_j} \int \mathrm{d}\boldsymbol{r} \prod_{u'=x,y,z} \psi^{n'_{u'}*}_{q'_{u'}}(u') \prod_{u=x,y,z} \psi^{n_u}_{q_u}(u) \\ =& \sum_{\boldsymbol{q}\boldsymbol{q}'} \frac{E^n_{\boldsymbol{q}}}{L^6} e^{i\boldsymbol{q}'\cdot\boldsymbol{r}_i} e^{-i\boldsymbol{q}\cdot\boldsymbol{r}_j} \delta_{\boldsymbol{q}\boldsymbol{q}'} \delta_{nn'} L^3 \\ =& \frac{1}{L^3} \sum_{\boldsymbol{q}} E^n_{\boldsymbol{q}} e^{i\boldsymbol{q}\cdot(\boldsymbol{r}_i - \boldsymbol{r}_j)} \end{aligned} \tag{2.39}$$

We observe that there is no amplitude to go between states that are in two different bands, as is indicated by the appereance of $\delta_{nn'}$. In what follows we will consider only the lowesrt band, $n = 0$, so we will drop the band index altogether. This simplification imposes two important requirements for our system:

1. The temperature and the Fermi energy need to be small compared to the energy gap between the lowest and first excited band.

2. The interaction energy scale must also be small comapred to the energy gap between the lowest and first excited band.

In the 3D lattice, the energy $E_{\boldsymbol{q}} = \sum_{u=x,y,z} E^u_{q_u}$, and by inserting this into the sum for

t_{ij} above we find

$$-t_{ij} = \frac{1}{L^3}\left[\left(\sum_{q_x} E^{\mathrm{1D}}_{q_x} e^{iq_x x_{ij}}\right)\sum_{q_y} e^{iq_y y_{ij}} \sum_{q_z} e^{iq_z z_{ij}} + \sum_{q_x} e^{iq_x x_{ij}}\left(\sum_{q_y} E^{\mathrm{1D}}_{q_y} e^{iq_y x_{ij}}\right)\sum_{q_z} e^{iq_z z_{ij}} + \sum_{q_x} e^{iq_x x_{ij}} \sum_{q_y} e^{iq_y y_{ij}}\left(\sum_{q_z} E^{\mathrm{1D}}_{q_z} e^{iq_z z_{ij}}\right)\right] \quad (2.40)$$

We make use of the identity $\sum_{q_x} e^{iq_x(x_i - x_j)} = L\delta_{x_i x_j}$, and similarly for y, z to obtain

$$-t_{ij} = \frac{1}{L}\left[\left(\sum_{q_x} E^{\mathrm{1D}}_{q_x} e^{iq_x x_{ij}}\right)\delta_{y_i y_j}\delta_{z_i z_j} + \left(\sum_{q_y} E^{\mathrm{1D}}_{q_y} e^{iq_y x_{ij}}\right)\delta_{x_i x_j}\delta_{z_i z_j} + \left(\sum_{q_z} E^{\mathrm{1D}}_{q_z} e^{iq_z z_{ij}}\right)\delta_{x_i x_j}\delta_{y_i y_j}\right] \quad (2.41)$$

We see that if $i = j$ we have

$$-t_{ii} = \frac{3}{L}\sum_{q} E^{\mathrm{1D}}_{q} \quad (2.42)$$

This contribution to H_0 just adds an overall energy (proportional to the number of particles in the system), so we just ignore it for convenience. Ignoring this term sets the zero of energy in the problem exactly at the center of the lowest band. This will be important in a later section, when we consider the phase diagram as a function of the chemical potential.

If on the other hand $i \neq j$, then we see that we can only consider the posibility that one of the x_{ij}, y_{ij}, z_{ij} is non-zero, otherwise all three of the terms in the expression above will vanish due to the Kronnecer delta terms. The expression for the tunneling matrix elements simplifies to

$$t_{ij} = -\frac{1}{L}\sum_{q} E^{\mathrm{1D}}_{q} e^{iq\Delta_{ij}} \quad (2.43)$$

where Δ_{ij} is the distance between sites at $\boldsymbol{r}_i$ and $\boldsymbol{r}_j$, and r_{ij} must be purely directed along x, y, or z. Also, as in the definition of the 1D Wannier states, the sum over q runs over the discrete values $q = \frac{2\pi n}{a}$ $\forall n \in \{0, 1, \ldots L-1\}$

We point out here that the tunneling matrix element can be computed directly from the integral

$$-t_{ij} = \int \mathrm{d}\boldsymbol{r}\, w_i(\boldsymbol{r}) H_{\mathrm{single,3D}} w_j(\boldsymbol{r}) \quad (2.44)$$

Numerical forms of the Wannier functions and their derivatives are easily obtained from the formulas in Sec. 2.1.3. Calculating the tunneling matrix element from the Wannier functions is computationally more expensive than obtaining it as a sum over the energy eigenvalues.

We observe from Eq. 2.43 that t_{ij} and E_q^{1D} are the Fourier series of one another, or in other words that the relation just shown can be inverted to obtain

$$E_q^{\mathrm{1D}} = -\sum_{\Delta_{ij}} t_{ij} e^{-iq\Delta_{ij}} \tag{2.45}$$

In the tight-binding approximation terms for which i, j are not nearest neighbors are neglected, and Δ_{ij} can only take the values $\{-a, a\}$. In this case we use $t_{ij} \equiv t$, and t satisfies

$$E_{q,\mathrm{tb}}^{\mathrm{1D}} = -2t\cos(qa) \tag{2.46}$$

This gives an expression that relates the bandwidth, W_{1D}, of the 1D lattice to the tunneling matrix element t

$$W_{\mathrm{1D}} = 4t. \tag{2.47}$$

In 3D this becomes $W_{\mathrm{3D}} = 12t$.

It is useful to find out the range of lattice depths for which the tight-binding approximation is valid in the optical lattice potential. To do this we just need to look at the tunneling matrix elements for beyond nearest-neighbor tunneling, this is shown in Fig. 2.7, which shows that for lattice depths $\gtrsim 5E_R$ we can safely ignore tunneling beyond nearest neighbors.

Another way of estimating the tunneling matrix element, suggested in [53], is by using the relationship $t = W_{\mathrm{1D}}/4$, valid in the tight-binding limit, and obtaining the bandwidth from the Mathieu functions, which are solutions to the Schrodinger equation in a 1D lattice. This yields the result

$$t \simeq \frac{4}{\sqrt{\pi}} V_0^{3/4} \exp(-2\sqrt{V_0}) \tag{2.48}$$

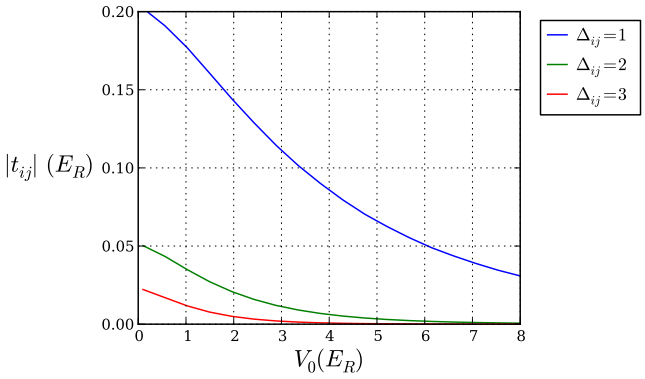

Figure 2.7: Tunneling matrix element in an optical lattice as a function of lattice depth. Nearest-neighbor and beyond nearest neighbor matrix elements are shown to illustrate the range of lattice depths for which the tight-binding limit is a good approximation. X_{ij} corresponds to the distance between intial and final site in the tunneling matrix element.

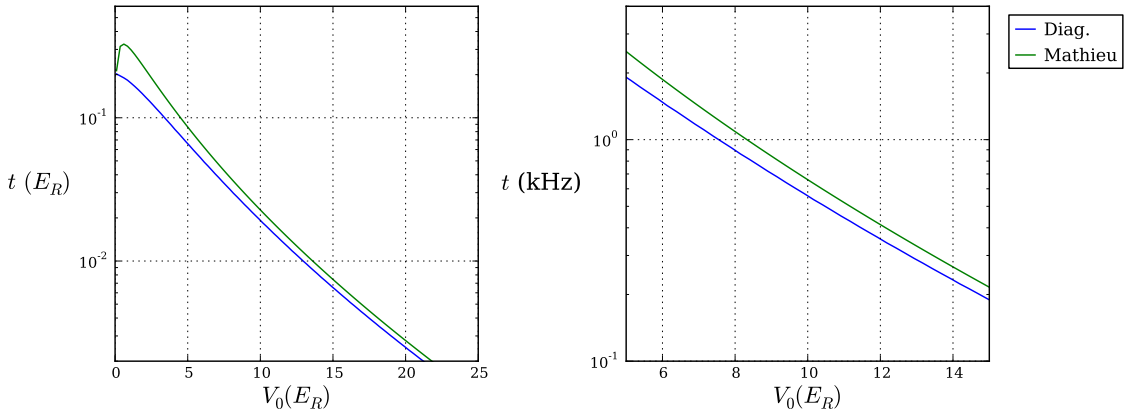

Figure 2.8: Nearest neighbor tunneling matrix element in an optical lattice as a function of lattice depth. Comparison between the result from Eq. 2.43 and the one obtained from the Mathieu functions. The right panel shows the tunneling rate in kHz for the mass of a ^{6}Li atom.

where t and V_0 are in units of the recoil energy. The comparision between the result from Eq. 2.43 and the result from the Mathieu functions is shown in Fig. 2.8.

Finally, we have the second quantized form of H_0 in the tight-binding limit

$$H_0 = -t \sum_{\langle ij \rangle} a_i^\dagger a_j \tag{2.49}$$

where the $\langle\rangle$ denote nearest-neighbors, and the creation operator $a_i^\dagger$ create particles in the Wannier state localized at site i.

Notice that up to now we have ignored the spin part of the wavefunction. We can include it easilly by noticing that H_0 does not act on the spin at all, so the states $|i\rangle$ and $|j\rangle$ that we have used in the derivation above need to have the same spin. With the spin included, our basis set is now larger which can be taken care of by including a sum over spin states.

$$H_0 = -t \sum_{\langle ij\rangle,\sigma=\uparrow\downarrow} a_{i\sigma}^\dagger a_{j\sigma} \tag{2.50}$$

On-site interaction energy, U The interaction part of the hamiltonian for N particles in a 3D lattice is given by

$$H_{\text{int}} = \frac{1}{2} \sum_{l,m,l\neq m}^{N} V_{\text{int}}(\boldsymbol{r}_l, \boldsymbol{r}_m) \tag{2.51}$$

This is a two-particle operator, and its second quantized form is given by

$$H_{\text{int}} = \frac{1}{2} \sum_{i,j,k,m} \langle ij|V_{\text{int}}|km\rangle a_i^\dagger a_j^\dagger a_m a_k \tag{2.52}$$

where

$$\langle ij|V_{\text{int}}|km\rangle = \int \mathrm{d}\boldsymbol{r}_1 \int \mathrm{d}\boldsymbol{r}_2 \;\; \varphi_i^*(\boldsymbol{r}_1)\varphi_j^*(\boldsymbol{r}_2)V_{\text{int}}(\boldsymbol{r}_1,\boldsymbol{r}_2)\varphi_k(\boldsymbol{r}_1)\varphi_m(\boldsymbol{r}_2) \tag{2.53}$$

The interaction between ultracold atoms can be described in terms of the s-wave scattering length, a, and a pseudopotential given by [53]

$$V_{\text{int}}(\boldsymbol{r}_1, \boldsymbol{r}_2) = \frac{4\pi\hbar^2 a}{m}\delta(\boldsymbol{r}_1 - \boldsymbol{r}_2) \tag{2.54}$$

so the matrix element above can be written as

$$\langle ij|V_{\text{int}}|km\rangle = \frac{4\pi\hbar^2 a}{m} \int \mathrm{d}\boldsymbol{r} \;\; \varphi_i^*(\boldsymbol{r})\varphi_j^*(\boldsymbol{r})\varphi_k(\boldsymbol{r})\varphi_m(\boldsymbol{r}) \tag{2.55}$$

Our basis states, φ, are the 3D Wannier states defined in Eq. 2.14, which are separable in the three spatial coordinates. We recall that the Wannier states are labeled by the lattice site on which they are centerend and by their band index. If we explicitly write out the two labels in the expression above we obtain

$$\langle ij|V_{\text{int}}|km\rangle = \frac{4\pi\hbar^2 a}{m} \prod_{v=x,y,z} \int \mathrm{d}v \;\; w_i^{n_i}(v) w_j^{n_j}(v) w_k^{n_k}(v) w_m^{n_m}(v) \tag{2.56}$$

The Wannier function along x, y, z depends on the lattice depth along the respective coordinate. We will consider a lattice with different depths along the three spatial coordinates, $\boldsymbol{V}_0 = (V_{0x}, V_{0y}, V_{0z})$. At this point we make the approximation of neglecting all of the off-site interaction terms, which can be justified by the localized nature of the Wannier states. Furthermore, we consider only Wannier states in the lowest band, which is valid for scattering lengths smaller than the single-site harmonic oscillator length [54]. With this considerations, and also explicitly writing down the spin quantum number, which so far was implicit in the indices $ijkm$, we find

$$\begin{aligned} H_{\text{int}} =& \frac{U}{2} \sum_{\sigma \neq \sigma'} \sum_i a_{i\sigma}^\dagger a_{i\sigma'}^\dagger a_{i\sigma'} a_{i\sigma} \\ =& \frac{U}{2} \sum_{\sigma \neq \sigma'} \sum_i n_{i\sigma'} n_{i\sigma} \\ =& U \sum_i n_{i\uparrow} n_{i\downarrow} \end{aligned} \tag{2.57}$$

where now i is an index that runs over lattice sites, and

$$U = \frac{4\pi\hbar^2 a}{m} \prod_{v=x,y,z} \int w(v)^4 \mathrm{d}v \tag{2.58}$$

In units of E_R,

$$U = \frac{8}{\pi} \frac{a_s}{a} \prod_{v=x,y,z} \int w(v)^4 \mathrm{d}v \tag{2.59}$$

where a is the lattice spacing.

If the Wannier state is approximated by the Gaussian ground state in the local oscillator potential of one lattice site, the integral can be carried out explicity and one gets [53]

$$U = \sqrt{8\pi} \frac{a_s}{a} V_0^{3/4} \tag{2.60}$$

where, again, the scattering length must be in units of the lattice spacing.

Alternatively we can use the Wannier states which were calculated in Sec. 2.1.3 and obtain a more accurate result. Figure 2.9 shows a comparison of the two methods for a lattice with $\lambda = 1064\,\text{nm}$.

If the scattering length is too large, and the on-site interaction term calculated here starts being comparable to the interband spacing then the single band approximation that

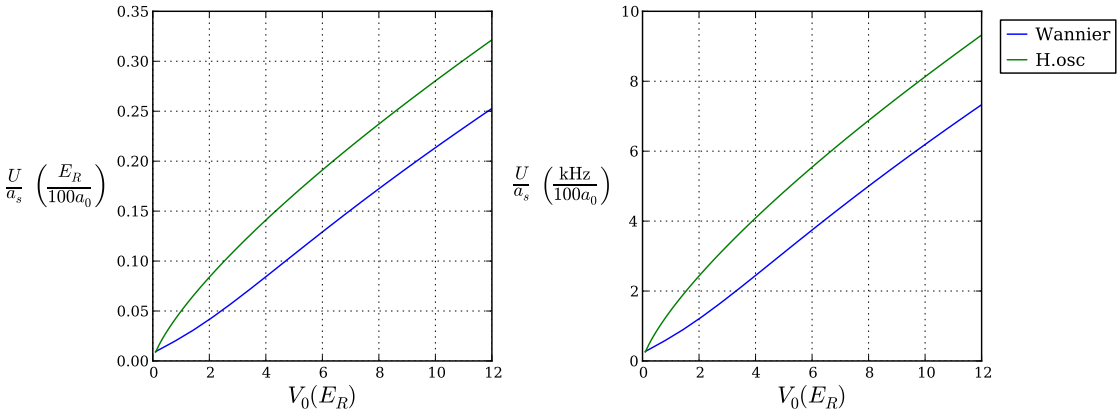

Figure 2.9: On-site interactions in a 3D lattice as a function of lattice depth. Numerical calculation using Wannier functions compeared to the approximation using harmonic oscillator states. The lattice depth is the same in all three directions of the lattice. The lattice wavelength is 1064 nm, and it is used to express the interactions in units of recoils divided by Bohr radius. The right panel shows it in kHz over Bohr radius for the mas of a ^{6}Li atom.

we introduced is no longer valid. One can treat the problem of two atoms inteacting in the local harmonic oscillator around a lattice site [54]. Another approach consists of redefining the single particle basis states (using linear combinations of Wannier states in different bands) such that the interaction matrix element is diagonal in the new basis, see for instance [55, 56]. In more formal terms one would find states

$$\varphi_i^{nm} = \sum_{st} c_{st}^{nm} w_i^s(\boldsymbol{r}) w_i^t(\boldsymbol{r}) \tag{2.61}$$

such that

$$\langle nm|V_{\text{int}}|op\rangle = \delta_{n,o}\delta_{m,p} \tag{2.62}$$

The problem of finding the coefficients c_{st}^{nm} can be tackled numerically by using linear combinations of Wannier states in only the first few bands.

2.3.4 Interactions between the atoms

approximate solutions to the Hubbard model are explained, including the high-temperature series expansion (HTSE) which is widely used throughout this thesis.

In this section I present the model in its original context, as a simplification of the description of valence electrons in crystalline solids. I include some historical background to motivate the reader.

Models for electrons existed which explained conduction phenomena in a succesful manner. Also, models existed which dealt with magnetic phenomena. This section touches on the necessity to formulate a model that could incorporate both transport and magnetic properties of a material. This need arises due to the existence of materials that are at neither end of the spectrum. That is, metals or insulators for which magnetic effects played an imporant role. The simple example being MnO, on which antiferromagnetism was first observed, and the big challenge being high-temperature superconductors.

3.1 Simplified treatements

This section explains our understanding of the Fermi-Hubbard model. It starts by building some insight by using the results of exactly solvable models. The results of exct diagonalization in systems of 2-sites and 4-sites are shown. This are going to motivate the antiferromagnetic character of the ground state, while showing that there is always a bit of an admixture of double occupancy in the exact ground state.

The 4-site solution can be used to help understand why the Fermi-Hubbard is relevant to high-Tc superconductors. In this case one can make connections to the d-wave character of ground states upon doping the system.

The exact diagonalization solutions are at zero temperature, so they give most insight to the exact ground states of the system.

3.1.1 Exact diagonalization

2 site exact diagonalization

4 site plaquete an relevance to high-Tc superconductors

3.1.2 Limiting cases

This section deals with the limiting cases of the Fermi-Hubbard parameters. The solutions that are obtained give insights to the workings of the model. The high temperature series expansion is introduced, which is very relevant for calculating thermodynamic quantitites in the temperature regime of a few times T_{Neel}.

U=0 limit, t=0 limit

3.1.3 High-temperature series expansion

In the atomic limit, where tunneling between sites is neglected completely, the Hubbard model can solved exactly. In this case the tunneling part of the hamiltonian can be treated as a perturbation and we can gain insight in to the different phases that the system can exhibit. This Section follows the treatment that can be found in [57, 55].

We work in the grand canonical ensemble, so we include a global chemical potential in the hamiltonian

$$\begin{aligned} H =& \left(U \sum_i n_{i\uparrow} n_{i\downarrow} - \mu \sum_i (n_{i\uparrow} + n_{i\downarrow}) \right) - t \sum_{\langle ij \rangle, \sigma} a^\dagger_{i\sigma} a_{j\sigma} \\ =& H_0 + H_1 \end{aligned} \tag{3.1}$$

For the unberturbed part, H_0, the grand canonical partition function is

$$Z_0 = \text{Tr} e^{-\beta H_0} \tag{3.2}$$

Since the unperturbed part is a sum over sites, the partition function becomes a product of the single site partition function, $Z_0 = z_0^k$, for a system with k sites. The single site partition function is easy to calculate because the trace runs over the only four possible

states in a single site $\{|0\rangle, |\uparrow\rangle, |\downarrow\rangle, |\updownarrow\rangle\}$.

$$z_0 = 1 + 2e^{\beta\mu} + e^{\beta(2\mu - U)} = 1 + 2z + z^2 u \tag{3.3}$$

where we have defined $z = e^{\beta\mu}$ and $u = e^{-\beta U}$. Among the relevant physical quantities that can be obtained are the number of particles, the number of double occupancies, and the entropy per site. These are obtained from the first derivatives of the grand canonical potential, Ω

$$\Omega = -\frac{\ln Z}{\beta} \tag{3.4}$$

$$N = -\frac{\partial \Omega}{\partial \mu} \tag{3.5}$$

$$D = \frac{\partial \Omega}{\partial U} \tag{3.6}$$

$$S = -\frac{\partial \Omega}{\partial T} \tag{3.7}$$

Also, from the second derivatives of the grand potential one can obtain the fluctuations in any of these quantitites.

For the full hamiltonian the grand canonical partition function Z can be expanded in a perturbation series [57]

$$\begin{aligned} Z =& \mathrm{Tr} e^{-\beta H} \\ =& Z_0 \left[1 + \sum_{n=1}^{\infty} (-1)^n \int_0^\beta d\tau_1 \int_0^{\tau_1} d\tau_2 \cdots \int_0^{\tau_{n-1}} d\tau_n \langle \tilde{H}_1(\tau_1) \tilde{H}_2(\tau_2) \cdots \tilde{H}_n(\tau_n) \rangle \right] \end{aligned} \tag{3.8}$$

where the thermal expectation value is taken with the unperturbed part of the hamiltonian

$$\langle A \rangle = \mathrm{Tr}(e^{\beta H_0} A)/Z_0 \tag{3.9}$$

and the tilde means that the operator is evaluated in the interaction picture for the imaginary time in parenthesis:

$$\tilde{H}_1(\tau) = e^{\tau H_0} H_1 e^{-\tau H_0} \tag{3.10}$$

Given the series expansion for Z, the grand potential is

$$-\beta\Omega = Z_0 + \sum_{n=1}^{\infty} (-1)^n \int_0^\beta d\tau_1 \int_0^{\tau_1} d\tau_2 \cdots \int_0^{\tau_{n-1}} d\tau_n \langle \tilde{H}_1(\tau_1) \tilde{H}_2(\tau_2) \cdots \tilde{H}_n(\tau_n) \rangle \tag{3.11}$$

One can see that the n^{th} term in the expansion has n copies of the tunneling part of the hamiltonian. Each application of H_1 in the thermal average results in a particle tunneling to a neighboring site, so we see that there will be a contribution to the expansion only if after n tunneling events all the particles come back to their original sites. A direct consequence of this is that the first order term in the expansion vanishes. The second order in the expansion corresponds to particles tunneling one site over and then coming back. Higher order terms can be represented by diagrams, to make them easier to keep track off. The contribution from orders up to $n = 9$ is shown in [57]. Here we will use up to the second order term to illustrate the phases that appear in the system.

The grand potential to second order is [57, 55]

$$-\beta\Omega_2 = k \ln z_0 + k \left(\frac{\beta t}{z_0}\right)^2 m \left(z + z^3 u + 2z^2 \frac{1-u}{\beta U}\right) \tag{3.12}$$

where m is the number of nearest neighbors for each lattice site, which in the simple cubic case is $m = 6$. We see that the grand potential is proportional to the number of lattice sites, so we will obtain all the thermodynamic quantities per lattice site.

The resulting phase diagram is shown in Fig. 3.1. NOTE FOR GROUP MEETING: I intend to write some text that discusses the relevant phases in this phase diagram. I will discuss them in the presentation in the group meeting and add the explanatory text in this document later on.

Thermodynamics at colder temperatures, apparoach to the Néel transition

In this section we show the phase diagram for the Fermi-Hubbard model at lower temperatures, which are beyond the scope of the perturbation expansion shown in the previous section. The phase diagram was calculated in [44] by using cluster dynamical mean-field theory, and they have made their results available in the supplementary material accompanying their paper. In Figures 3.2,3.3,3.4 we show the resulting phase diagram for $T/t = 10$, 1, and 0.3 respectively.

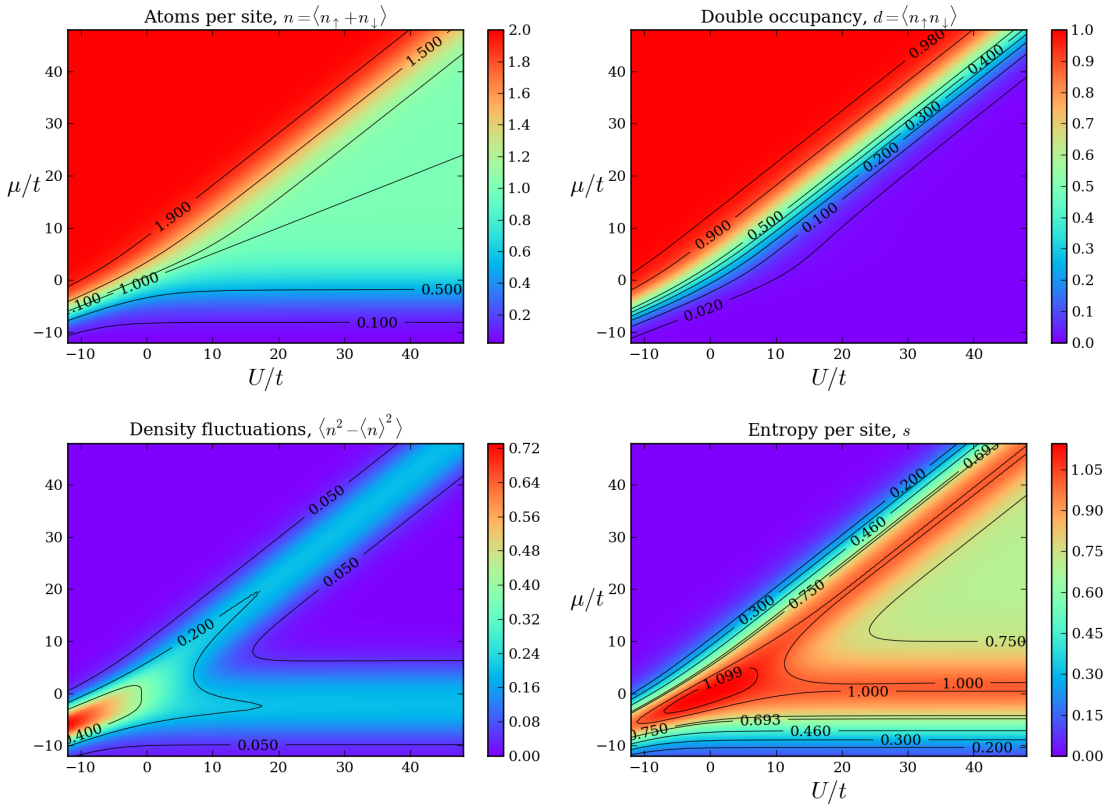

Figure 3.1: High temperature phase diagram of the Fermi-Hubbard model calculated using only the second order in the perturbation series.

3.1.4 Local density approximation

The phase diagrams calculated in the two previous sections assume a homogeneous lattice. In our experiment the lattice has an underlying confining potential, which can be dealt with by considering a local chemical potential at each point in the trap given by

$$\mu(\boldsymbol{r}) = \mu - V(\boldsymbol{r}) \tag{3.13}$$

An homogeneous lattice phase diagram can be used to obtain the local density, local entropy, and local double occupancy at any point in our system by using as inputs the local chemical potential, the local value of the tunneling matrix element and the local value of the on-site interaction.

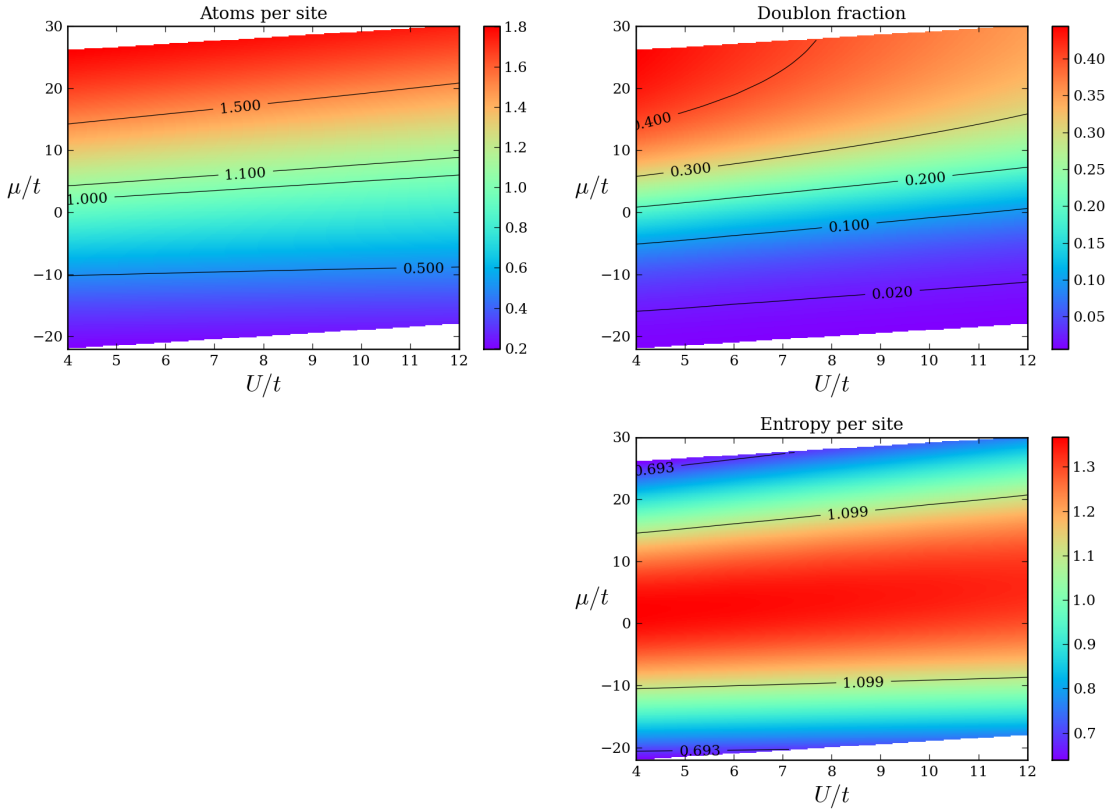

Figure 3.2: From [44]

The methods used to calculate the phase diagrams are related to the validity of the local density approximation. We recall that in the high temperature series expansion, the n^{th} term corresponds to a particle staring at a certain site, tunneling n times and then coming back to its original site. If $\sqrt{n}$ becomes comparable to the lenght scale of variations in the confining potential, then the local density would not be a suitable description of the system, because in those n steps the particle can sample a very different confining potential.

Similarly, in the cluster dynamical mean-field theory, results are obtained for finite sized clusters of various sizes and then extrapolated to the infinite size limit [44]. At low temperatures, the system develops long-range correlations, so large clusters are required to approximate the system. If the local site energy varies considerably over the size of a cluster then the local density approximation will break down.

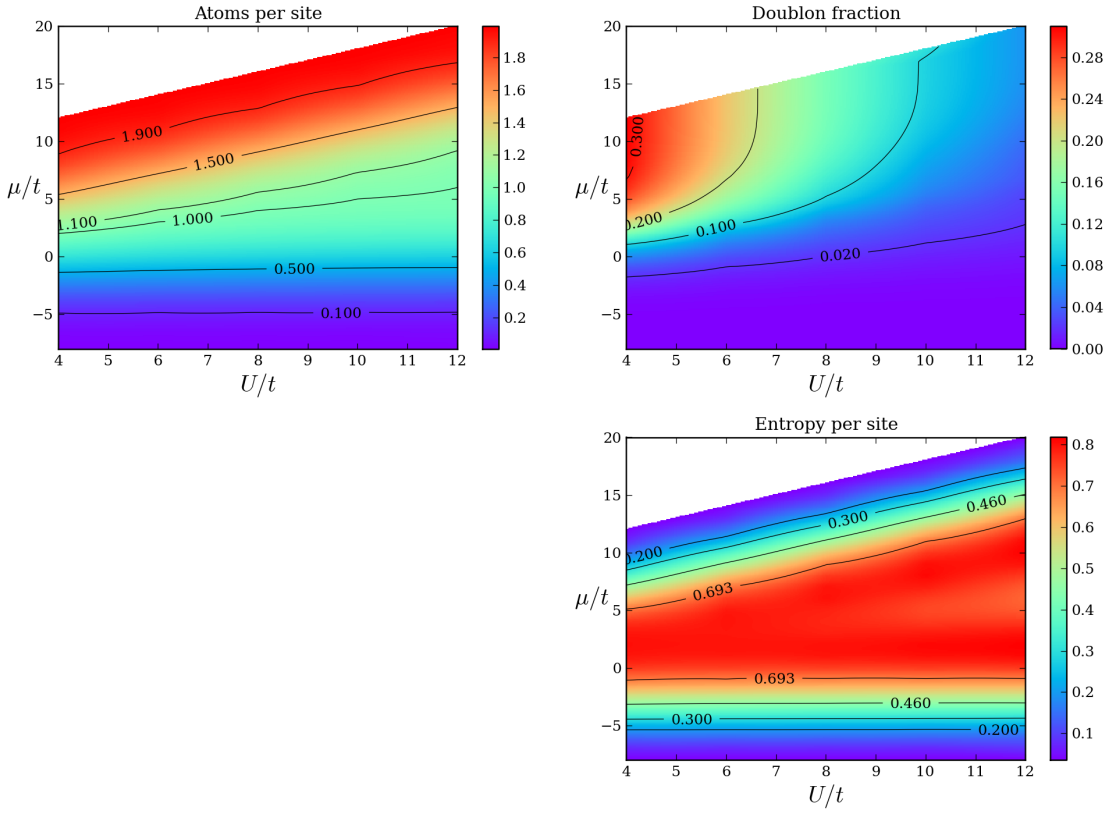

Figure 3.3: From [44]

High temperature series expansion, band and Mott insulating states

small t, the t-J model and antiferromagnetic ground state

3.1.5 Modern approaches

This small section aims to explain the most recente advances in our understanding the Fermi-Hubbard model. This includes QMC, DMFT, etc. The aim of this section is not to provide an introduction to these techniques but mainly to point out the main results and serve as a bibliographic reference.

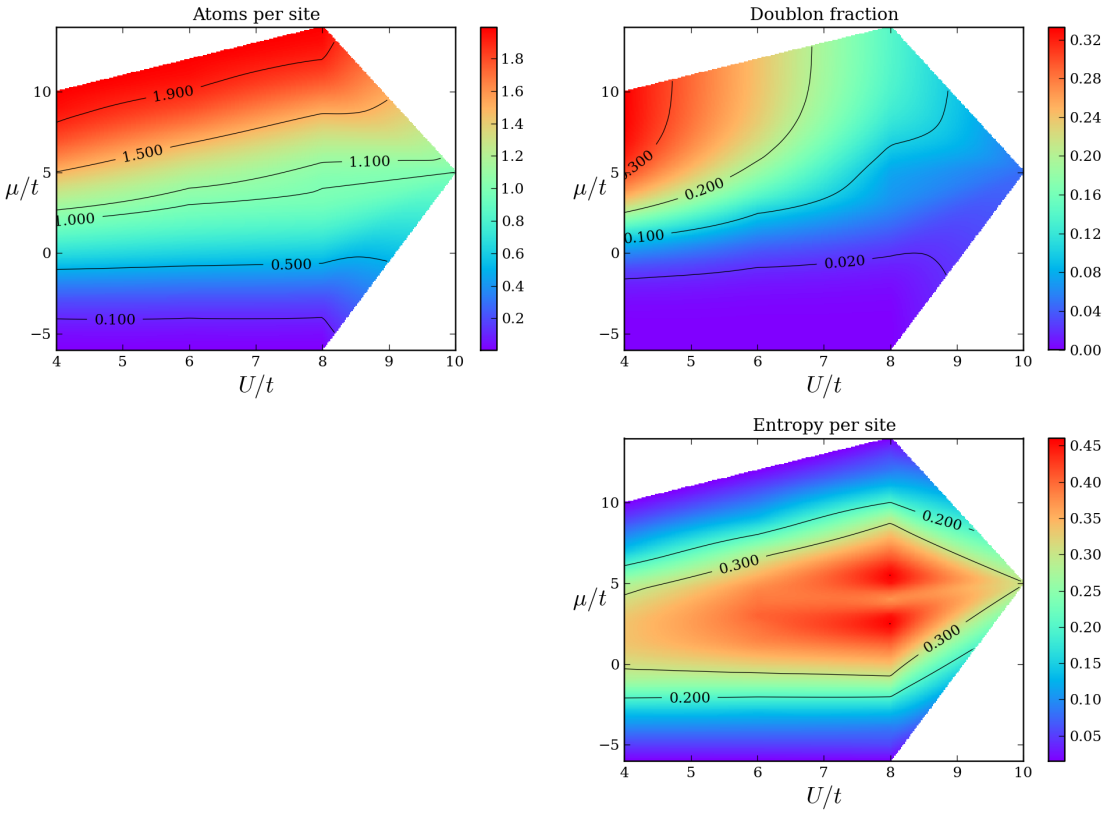

Figure 3.4: From [44]

Enlarging and cooling towards the Neel state in a compensated optical lattice potential

4.1 Compensated optical lattice
4.2 Thermodynamic quantitites in the local density approximation

This chapter aims to describe in detail the different observables that are accesible to the experimetnalist.

5.1 Absorption imaging
5.2 Polarization phase-contrast imaging
5.3 Thermometry of a Fermi gas trapped in a harmonic potential
5.4 Double occupancy measurement in an optical lattice
5.5 Bragg Scattering of light
5.5.1 Non-spin sensitive: crystal structure factor
5.5.2 Spin sensitive: spin-structure factor

6.1 Production of a deeply degenerate ^{6}Li spin mixture in a dimple potential
6.2 Compensated optical lattice potential

7.1 Determination of the crystal structure factor using Bragg scattering
7.2 Insulating states in an uncompensated lattice
7.3 Evaporative cooling in a compensated optical lattice
7.4 Detection of antiferromagnetic correlations in a compensated optical lattice

Conclusion

BIBLIOGRAPHY

[1] X. Wen, *Quantum Field Theory of Many-Body Systems: From the Origin of Sound to an Origin of Light and Electrons*, *Oxford Graduate Texts* (OUP Oxford, 2004).

[2] A. Altland and B. Simons, *Condensed Matter Field Theory* (Cambridge University Press, 2010).

[3] N. Ashcroft and N. Mermin, *Solid state physics*, *Science: Physics* (Saunders College, 1976).

[4] L. Landau, *Collected papers of L. D. Landau* (Gordon and Breach, 1965).

[5] K. Andres, J. E. Graebner, and H. R. Ott, "¡span class=”aps-inline-formula”¿¡math¿¡mn¿4¡/mn¿¡mi¿f¡/mi¿¡/math¿¡/span¿-Virtual-Bound-State Formation in Ce¡span class=”aps-inline-formula”¿¡math¿¡mrow¿¡msub¿¡mrow¿¡mi mathvariant=”normal”¿Al¡/mi¿¡/mrow¿¡mrow¿¡mn¿3¡/mn¿¡/mrow¿¡/msub¿¡/mrow¿¡/math¿¡/span¿ at Low Temperatures," Phys. Rev. Lett. **35,** 1779–1782 (1975).

[6] F. Steglich, J. Aarts, C. D. Bredl, W. Lieke, D. Meschede, W. Franz, and H. Schäfer, "Superconductivity in the Presence of Strong Pauli Paramagnetism: Ce¡span class=”aps-inline-formula”¿¡math¿¡mrow¿¡msub¿¡mrow¿¡mi mathvariant=”normal”¿Cu¡/mi¿¡/mrow¿¡mrow¿¡mn¿2¡/mn¿¡/mrow¿¡/msub¿¡/mrow¿¡/math¿¡/span¿¡span class=”aps-inline-formula”¿¡math¿¡mrow¿¡msub¿¡mrow¿¡mi mathvariant=”normal”¿Si¡/mi¿¡/mrow¿¡mrow¿¡mn¿2¡/mn¿¡/mrow¿¡/msub¿¡/mrow¿¡/math¿¡/span¿," Phys. Rev. Lett. **43,** 1892–1896 (1979).

[7] D. C. Tsui, H. L. Stormer, and A. C. Gossard, "Two-Dimensional Magnetotransport in the Extreme Quantum Limit," Phys. Rev. Lett. **48,** 1559–1562 (1982).

[8] R. B. Laughlin, "Anomalous Quantum Hall Effect: An Incompressible Quantum Fluid with Fractionally Charged Excitations," Phys. Rev. Lett. **50,** 1395–1398 (1983).

[9] J. Bednorz and K. MÃijller, "Possible highT c superconductivity in the BaâĹŠLaâĹŠCuâĹŠO system," Zeitschrift fÃijr Physik B Condensed Matter **64,** 189–193 (1986).

[10] P. Coleman, "Many Body Physics: Unfinished Revolution," in *International Conference on Theoretical Physics*, D. Iagolnitzer, V. Rivasseau, and J. Zinn-Justin, eds., (BirkhÃďuser Basel, 2004), pp. 559–580.

[11] P. W. Anderson, "More Is Different," Science **177,** 393–396 (1972).

[12] X. G. WEN, "Topological orders in rigid states," International Journal of Modern Physics B **04,** 239–271 (1990).

[13] J. A. Hertz, "Quantum critical phenomena," Phys. Rev. B **14,** 1165–1184 (1976).

[14] S. Sachdev, *Quantum Phase Transitions*, *Quantum Phase Transitions* (Cambridge University Press, 2011).

[15] J. Quintanilla and C. Hooley, "The strong-correlations puzzle," Physics World **22,** 32–37 (2009).

[16] D. Jaksch, C. Bruder, J. I. Cirac, C. W. Gardiner, and P. Zoller, "Cold Bosonic Atoms in Optical Lattices," Phys. Rev. Lett. **81,** 3108–3111 (1998).

[17] R. P. Feynman, "Simulating physics with computers," International journal of theoretical physics **21,** 467–488 (1982).

[18] M. Greiner, O. Mandel, T. Esslinger, T. Hänsch, and I. Bloch, "Quantum phase transition from a superfluid to a Mott insulator in a gas of ultracold atoms," Nature pp. 39–44 (2002).

[19] N. Gemelke, X. Zhang, C.-L. Hung, and C. Chin, "In situ observation of incompressible Mott-insulating domains in ultracold atomic gases.," Nature **460,** 995–8 (2009).

[20] K. Jiménez-García, R. L. Compton, Y.-J. Lin, W. D. Phillips, J. V. Porto, and I. B. Spielman, "Phases of a Two-Dimensional Bose Gas in an Optical Lattice," Physical Review Letters **105,** 110401 (2010).

[21] S. Trotzky, L. Pollet, F. Gerbier, U. Schnorrberger, I. Bloch, N. V. ProkofâĂŹev, B. Svistunov, and M. Troyer, "Suppression of the critical temperature for superfluidity near the Mott transition," Nature Physics **6,** 998–1004 (2010).

[22] M. J. Mark, E. Haller, K. Lauber, J. G. Danzl, a. J. Daley, and H.-C. Nägerl, "Precision Measurements on a Tunable Mott Insulator of Ultracold Atoms," Physical Review Letters **107,** 175301 (2011).

[23] X. Zhang, C.-L. Hung, S.-K. Tung, and C. Chin, "Observation of quantum criticality with ultracold atoms in optical lattices.," Science (New York, N.Y.) **335,** 1070–2 (2012).

[24] J. K. Freericks and H. Monien, "Phase diagram of the Bose-Hubbard Model," EPL (Europhysics Letters) **26,** 545 (1994).

[25] W. Krauth and N. Trivedi, "Mott and Superfluid Transitions in a Strongly Interacting Lattice Boson System," EPL (Europhysics Letters) **14,** 627 (1991).

[26] M. P. A. Fisher, P. B. Weichman, G. Grinstein, and D. S. Fisher, "Boson localization and the superfluid-insulator transition," Phys. Rev. B **40,** 546–570 (1989).

[27] T. Fukuhara, P. Schauß, M. Endres, S. Hild, M. Cheneau, I. Bloch, and C. Gross, "Microscopic observation of magnon bound states and their dynamics.," Nature **502,** 76–9 (2013).

[28] M. Köhl, H. Moritz, T. Stöferle, K. Günter, and T. Esslinger, "Fermionic Atoms in a Three Dimensional Optical Lattice: Observing Fermi Surfaces, Dynamics, and Interactions," Physical Review Letters **94,** 080403 (2005).

[29] R. Jördens, N. Strohmaier, K. Günter, H. Moritz, and T. Esslinger, "A Mott insulator of fermionic atoms in an optical lattice.," Nature **455,** 204–7 (2008).

[30] U. Schneider, L. Hackermüller, S. Will, T. Best, I. Bloch, T. A. Costi, R. W. Helmes, D. Rasch, and A. Rosch, "Metallic and insulating phases of repulsively interacting fermions in a 3D optical lattice.," Science (New York, N.Y.) **322,** 1520–5 (2008).

[31] A. Damascelli, Z. Hussain, and Z. Shen, "Angle-resolved photoemission studies of the cuprate superconductors," Reviews of Modern Physics 75 (2003).

[32] R.-H. He *et al.*, "From a single-band metal to a high-temperature superconductor via two thermal phase transitions.," Science (New York, N.Y.) **331,** 1579–83 (2011).

[33] K. Jin, N. P. Butch, K. Kirshenbaum, J. Paglione, and R. L. Greene, "Link between spin fluctuations and electron pairing in copper oxide superconductors.," Nature **476,** 73–5 (2011).

[34] P. M. Grant, "High-temperature superconductivity: The great quantum conundrum.," Nature **476,** 37–9 (2011).

[35] J. Milton, "Superconductors come of age,", Nature News. doi:10.1038/news.2010.527, 2010.

[36] M. Wu, J. Ashburn, C. Torng, and P. Hor, "Superconductivity at 93 K in a new mixed-phase Y-Ba-Cu-O compound system at ambient pressure," Physical Review ... **58,** 908–910 (1987).

[37] J. Tranquada *et al.*, "Antiferromagnetism in YBa2Cu3O(6+x)," Physical Review B **38,** 2477–2485 (1988).

[38] L. Liáng, *YBCO Superconductor Research Progress* (Nova Science Publishers, 2008).

[39] M. Köhl, "Thermometry of fermionic atoms in an optical lattice," Physical Review A **73,** 031601 (2006).

[40] E. Koch, in *Correlated Electrons: From Models to Materials*, E. Pavarini, E. Koch, F. Anders, and M. Jarrell, eds., (Forschungszentrum JÃijlich GmbH, Julich, Germany, 2012), Chap. Exchange mechanisms.

[41] D. Greif, T. Uehlinger, G. Jotzu, L. Tarruell, and T. Esslinger, "Short-Range Quantum Magnetism of Ultracold Fermions in an Optical Lattice," Science 1307 (2013).

[42] S. Trotzky, P. Cheinet, S. Fölling, M. Feld, U. Schnorrberger, a. M. Rey, a. Polkovnikov, E. a. Demler, M. D. Lukin, and I. Bloch, "Time-resolved observation and control of superexchange interactions with ultracold atoms in optical lattices.," Science (New York, N.Y.) **319,** 295–9 (2008).

[43] T. Paiva, Y. L. Loh, M. Randeria, R. T. Scalettar, and N. Trivedi, "Fermions in 3D Optical Lattices: Cooling Protocol to Obtain Antiferromagnetism," Physical Review Letters **107,** 086401 (2011).

[44] S. Fuchs, E. Gull, L. Pollet, E. Burovski, E. Kozik, T. Pruschke, and M. Troyer, "Thermodynamics of the 3D Hubbard Model on Approaching the Néel Transition," Physical Review Letters **106,** 030401 (2011).

[45] E. L. Jr, J. Gubernatis, and R. Scalettar, "Sign problem in the numerical simulation of many-electron systems," Physical Review B **41,** 9301–9307 (1990).

[46] D. C. McKay and B. DeMarco, "Cooling in strongly correlated optical lattices: prospects and challenges," Reports on Progress in Physics **74,** 054401 (2011).

[47] O. Morsch and M. Oberthaler, "Dynamics of Bose-Einstein condensates in optical lattices," Rev. Mod. Phys. **78,** 179–215 (2006).

[48] J. C. Slater, "A Soluble Problem in Energy Bands," Phys. Rev. **87,** 807–835 (1952).

[49] C. Salomon, G. Shlyapnikov, and L. Cugliandolo, *Many-Body Physics with Ultracold Gases: Lecture Notes of the Les Houches Summer School: Volume 94, July 2010*, *Lecture Notes of the Les Houches Summer School* (OUP Oxford, 2013).

[50] W. Kohn, "Analytic Properties of Bloch Waves and Wannier Functions," Physical Review **115,** 809–821 (1959).

[51] A. Fetter and J. Walecka, *Quantum Theory of Many-particle Systems*, *Dover Books on Physics* (Dover Publications, 2003).

[52] F. Schwabl, *Advanced Quantum Mechanics*, *Advanced texts in physics* (Springer, 2005).

[53] I. Bloch and W. Zwerger, "Many-body physics with ultracold gases," Reviews of Modern Physics **80,** 885–964 (2008).

[54] T. Busch, B. Englert, K. RzaÅijewski, and M. Wilkens, "Two cold atoms in a harmonic trap," Foundations of Physics pp. 549–559 (1998).

[55] R. Jördens, Ph.D. thesis, ETH Zürich, 2010.

[56] M. Mark, Ph.D. thesis, Innsbruck, 2012.

[57] J. Henderson, J. Oitmaa, and M. Ashley, "High-temperature expansion for the single-band Hubbard model," Physical Review B **46,** 6328–6337 (1992).